Article

Impact Assessments of Rainfall–Runoff Characteristics Response Based on Land Use Change via Hydrological Simulation

Minmin Zhou [1,3], Simin Qu [1,2], Xueqiu Chen [2], Peng Shi [1,2,*], Shijin Xu [4], Hongyu Chen [4], Huiyan Zhou [2] and Jianfeng Gou [2]

[1] State Key Laboratory of Hydrology-Water Resources and Hydraulic Engineering, Hohai University, Nanjing 210098, China; minmin_miao@163.com (M.Z.); wanily@hhu.edu.cn (S.Q.)

[2] College of Hydrology and Water Resources, Hohai University, Nanjing 210098, China; cxqhhu@163.com (X.C.); huiyanZ@126.com (H.Z.); jf_gou@sina.com (J.G.)

[3] Hohai University Design Institude CO., Ltd. Shanghai Branch, Shanghai 200000, China

[4] Hydrological Bureau, The Huai River Commission of the Ministry of Water Resources, Bengbu 233040, China; sjxu@hrc.gov.cn (S.X.); hychen1@hrc.gov.cn (H.C.)

* Correspondence: ship@hhu.edu.cn; Tel.: +86-138-1307-7076

check for
updates

Abstract: The hydrology response was studied considering the established fact of land use change in Dapoling basin. The whole period was divided into two (1965–1985 and 1986–2012) according to the major land use and land cover change in this region. Xinanjiang model was used to simulate discharge data in the two periods. The hydrologic response to the change could be evaluated by inspecting the response of model parameters and flood elements. The results show that the lag time varied, and the hydrologic elements including the mean runoff depth, flood peak and kurtosis coefficient varied with the rainfall depth. This result is significant for studying the response of runoff characteristic from land use and land cover change.

1. Introduction

Land use and land cover patterns change dramatically with the expansion of human activities, the impact of which on environment and sustainable development has attracted widespread attention [1–4]. The mechanism of hydrologic process is complex, which relates not only to the spatial and temporal distribution of basin physiographic factors, but also to the basin's underlying surface conditions. Vörösmarty [2] showed that land use change and climate change are two factors that impact hydrology. On a long time scale, climate change impacts more than land use change. However, on a short time scale, land use change impacts more. The existing research [5–7] shows that the major land use variations that affect hydrology are afforestation and deforestation. Other significant factors influencing hydrology include agricultural development, wetland drainage, urbanization, land abandonment and changes due to forest fire. The immediate and direct impacts of these land use changes on water yield and water quality of basin runoff are multiple and different in temporal and spatial scale [5].

The hydrologic response to land use change reveals that land use change alters elements such as evapotranspiration [8,9], runoff depth [10,11], mean annual runoff [12–14], snowmelt [1,15], soil erosion [16,17] and the groundwater quality [18] to affect overall basin hydrology. It is well documented that land use change therefore can have a significant effect on river basin hydrology, which is mainly reflected on the change of the flood volume [1,9], peak flow discharge [10,13], flood frequency [19] and peak flow rate [20]. De Roo et al. [21] explored the impact of land use change on flood in

the Oder (The Czech Republic, Poland and Germany) and Meuse (France, Belgium, Germany, and The Netherlands) basins based on the distributed hydrological model LISFLOOD, which was developed by the flood group of the Natural Hazards Project of the Joint Research Centre of the European Commission. They concluded that the overall effects during the period experiencing land use change are: the flood risk of the basin tends to increase, soil storage capacity has decreased 12 mm before flood comes, the flood peak discharge has increased 0.2%, and water level has increased 1 cm. Mao et al. [22] studied the hydrologic response of land use change in the Great Lakes region of America using the Variable Infiltration Capacity (VIC) model. At regional scales, the simulated results due to land use change vary spatially and seasonally, which is largely related to vegetation conversion and the geographic location of each land use type. Compared to the condition before land use change, the deforestation and conversion of deciduous forest into woodland and row-crop agriculture in the research center leads to a reduced evapotranspiration and the increased total runoff; the conversion of majority evergreen into majority deciduous forest in the northern part leads to a reduced evapotranspiration and the increased total runoff; and the conversion of prairie grasslands into row agriculture in the southern and western part leads to an increased evapotranspiration and the reduced total runoff. In addition, the land degradation and vegetation cover changes affect soil quality [18]. The authors [18] found that deforestation and agricultural expansion have significant impact on groundwater quality in Northern Kelantan, Malaysia. They tested the nitrate values and found that the concentrations show a significant positive trend in both the agricultural and residential wells, while forests and grasslands show an annual decrease.

Lag time is a fundamental descriptor of basin characteristics, reflecting the time difference between the rainfall and the resulting hydrograph [23]. It is a comprehensive index related with some internal processes of the catchment and gives the information of the water storage, flow path, water resources quantity and concentration time. The calculation of lag time can reflect the information of the time of flood peak discharge, which is important for basin flood management. Lag time is the fingerprint of water that reflects the physiography and flow routing of basin, which changes conspicuously with the change of basin land surface [24]. Previous research on lag time mainly considered the estimation of flood peak and the hydrograph shape [25,26], the comparison of the variation of slope flow and river flow [27], the impact of different urbanization degree on lag time [23,24,28], and the basis of choosing a flood event for rainfall–runoff model [29,30].

Recently, the studies of land use change in the Huai River basin mainly focused on runoff generation process [31], evapotranspiration [32], water yield [33,34], rainfall–runoff relationship [33], water quality [35], pollution characteristics [36] and sediment yield characteristics [37]. Research on the impact of land use change on basin lag time in the Huai River basin is scarce. More understanding of the influence of land use change on lag time can provide guiding significance for flood forecasting and water resources management of the basin. Determining the lag time of a basin can provide significant guidance for forecasting the time of peak discharge for this basin and the downstream basins, which makes the search meaningful.

Based on previous studies and the available data of hydrology and land use, we chose Dapoling basin for this research. The land use change is an established fact of the selected basin. The mechanism of how land use change influences the hydrology has been widely discussed in other studies, thus the object of this research was to test the hydrology response based on the fact of land use change and provide guidance for flood forecasting. Dapoling basin is the head source of Huai River. Its hydrology condition is important for downstream basins.

2. Materials

2.1. Study Area

The authors of [38,39] used a detection method based on hydrology model to test the hydrology response to land use change in Xixian basin. Our study area was the head source sub-basin of Xixian. The sub-basin Dapoling is located in the upstream of the Huai River at the latitudes 113°16′04″E to

113°49′26″E, and longitudes 32°13′01″N to 32°43′05″N, as shown in Figure 1. The length of the main channel in Dapoling basin is about 73 km and the area is 1640 km^2, covered with various vegetation growing well. The Dapoling basin is located in the transition zone between subtropical zone and temperate zone, and is heavily affected by the monsoon climate in the flood season. The perennial average evaporation is about 1000 mm in the region and the annual average temperature is between 11 °C and 16 °C. The main soil types of the basin are light silty loam and sandy loam soil, and part is underlain by silt clay. Rice and wheat are the main crops grown in the area. Dapoling basin is the head source of the Huai River. Most of the basin is covered by Dabie Mountain. The rivers flow over a mountainous terrain with many tributaries and large slope. There are no reservoirs in the river.
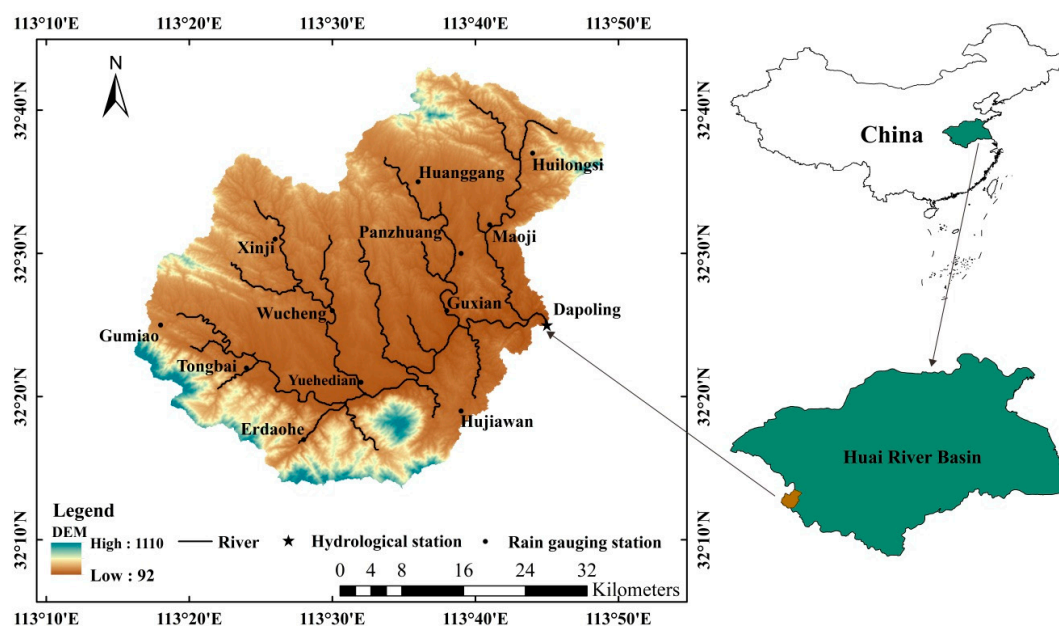

Figure 1. The study area of Dapoling basin.

The rainfall station of Dapoling basin is shown in Table 1 and Figure 1. According to the observed data in Table 1, the maximum water level stage is 104.86 m and the corresponding maximum discharge is 4200 m^3/s at Dapoling station. The mean annual precipitation is 918 mm (derived from 1964 to 2005), half of which falls between June and September. The mean annual runoff depth is 375 mm.

Table 1. The data and stations of Dapoling basin.

Station Type	Station Code	Station Name	The Maximum Rainfall (mm)	The Maximum Discharge (m^3/s)
Rainfall station	82001	Gumiao	264.9	-
	82002	Tongbai	365.1	-
	82003	Erdaohe	302.5	-
	82004	Xinji	326.5	-
	82005	Wucheng	275.2	-
	82006	Yuehedian	343.3	-
	82007	Huanggang	246.2	-
	82008	Panzhuang	245.2	-
	82009	Guxian	225.6	-
	82010	Hujiawan	324.2	-
	82011	Huilongsi	212.3	-
	82012	Maoji	211.6	-
Hydrology station	82013	Dapoling	254.1	4200
Mean annual precipitation of the basin (mm)				918
Mean annual runoff depth of the basin (mm)				375

2.2. Land Use Data

The land use data are from Resource and Environment Data Cloud Platform of Chinese Academy of Sciences (Table 2 and Figure 2). The data show that the main land use type in the basin are farmland and woodland, accounting for 41.85% and 38.55% in the 1980s, 30.38% and 40.68% in the 1990s, and 41.81% and 38.06% in the 2000s, respectively. The principal variation is the cross change of farmland and paddy field. Compared with the 1990s, the paddy field reduced to 17.15% from 27.23%, and the farmland increased to 41.81% from 30.38%. Compared with the 1980s, the paddy field increased to 27.23% from 17.02%, and the farmland reduced to 30.38% from 41.85%.

Table 2. The land use data for three periods in the basin.

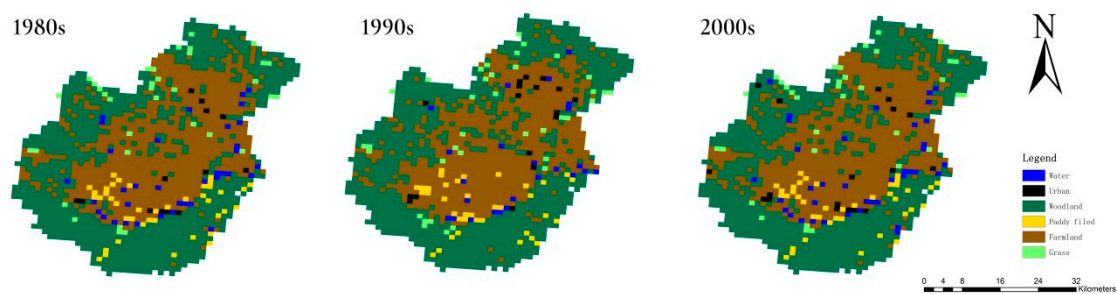| Land Use	Proportion (%)		
	1980s	**1990s**	**2000s**
Water	0.9	0.78	1.32
Urban	0.63	0.51	0.88
Woodland	38.55	40.69	38.06
Paddy filed	17.02	27.23	17.15
Farmland	41.85	30.38	41.81
Grass	0.57	0.06	0.54

Figure 2. The land use type of the three periods.

3. Methods

3.1. Xinanjiang Model

A physically-based hydrological model is an important tool for hydrology research and water resources management [40]. Many hydrological models have been developed and applied to watersheds with various sizes. The Xinanjiang Model is widely used in China. It was developed by Zhao in 1973 (Hohai University, China) [41]. The model is extensively used for runoff simulation in humid and semi-humid basins in China and has achieved high accuracy. The Xinanjiang Model is workable for variable input data from the minute scale to the daily scale and calculates the outflow at the corresponding time scale. Thus, it is suitable for calculating the flood discharge in small and medium watersheds with flood propagation time less than 24 h. The input data of Xinanjiang Model are mainly the rainfall and evaporation data. It does not consider Digital Elevation Model (DEM) data. Comparing to other distributed hydrological models, which need geographic data, Xinanjiang model only demands hydrology data, which makes the model easy to use.

Considering the uneven distribution of rainfall and the underlying surface, the study basin is divided into several sub-units by the Thiessen polygon method in ArcGIS [42]. The method assumes that the data of rainfall station located at the center of each Thiessen polygon could represent the areal mean rainfall in sub-units.

The evapotranspiration, the runoff production, the separation of runoff components and the flow concentration of hill slope are first simulated separately in each divided sub-unit successively, and then flood routing down the channels from the sub-unit outlets to the main basin outlet is obtained by applying the Muskingum method.

The main characteristic of the model is the concept of runoff formation on repletion of storage, which means that runoff will not be produced until the soil moisture content of aeration zone reaches the field capacity, and thereafter the total runoff equals to the total rainfall. To describe the non-uniform distribution of tension water capacity in sub-basins, a tension water capacity curve is introduced (Figure 3):

$$f/F = 1 - (1 - W'/WMM)^B \tag{1}$$

where f represents the area of runoff production; F represents the area of basin; W' represents the tension water capacity at a point; and WMM is the maximum value of W'. The areal mean tension water capacity, WM, is easy to obtain from Equation (2) by integration. B is the parameter shown in Table 3.

$$WM = WMM/(1 + B) \tag{2}$$

$$\text{If } P - KC \times EM + A < WMM,$$
$$\text{then } R = P - KC \times EM - WM + W_0 + WM \times [1 - (P - KC \times EM + A)/WMM]^{1+B} \tag{3}$$
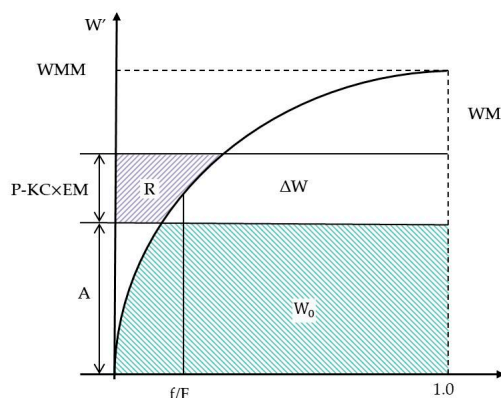

Figure 3. The tension water capacity curve in Xinanjiang Model.

Otherwise

$$R = P - KC \times EM - WM + W_0 \tag{4}$$

where P is the measured areal mean rainfall; EM is the measured pan evaporation; A is the ordinate value corresponding to WM; R is the runoff depth produced from permeable area; W_0 is the initial tension water storage of sub-basin; and KC and WM are parameters shown in Table 3.

The Muskingum method is based on the principle of water balance and the relation of storage and outflow. It has two basic assumptions. One is that the water level is a straight line and flow varies linearly along the reach. The other is that there is a single relationship between the discharge Q at a section and the storage W in the river.

The water balance equation is as follows:

$$I - Q = dW/dt \tag{5}$$

where I is the inflow, Q is the outflow, W is the storage amount, and t is the computation time.

The channel storage equation as follows:

$$W = f(I,Q) \tag{6}$$

The flow proportion coefficient XE and the slope of the channel storage curve KE are used in the equation set. The flow routing equation can be obtained by solving the equation set, as below:

$$Q_2 = C_0 \times I_2 + C_1 \times I_1 + C_2 \times Q_1 \tag{7}$$

$$C_0 = \frac{0.5\Delta t - KE\cdot XE}{0.5\Delta t + KE - KE\cdot XE}, \quad C_1 = \frac{0.5\Delta t + KE\cdot XE}{0.5\Delta t + KE - KE\cdot XE}, \quad C_2 = \frac{-0.5\Delta t + KE - KE\cdot XE}{0.5\Delta t + KE - KE\cdot XE} \tag{8}$$

where C_0, C_1, and C_2 are coefficients with the relationship:

$$C_0 + C_1 + C_2 = 1 \tag{9}$$

The structure of the Xinanjiang model is presented in Figure 4. The model parameters and the intermediate variables are displayed in Tables 3 and 4.

Table 3. Parameters in Xinanjiang model.

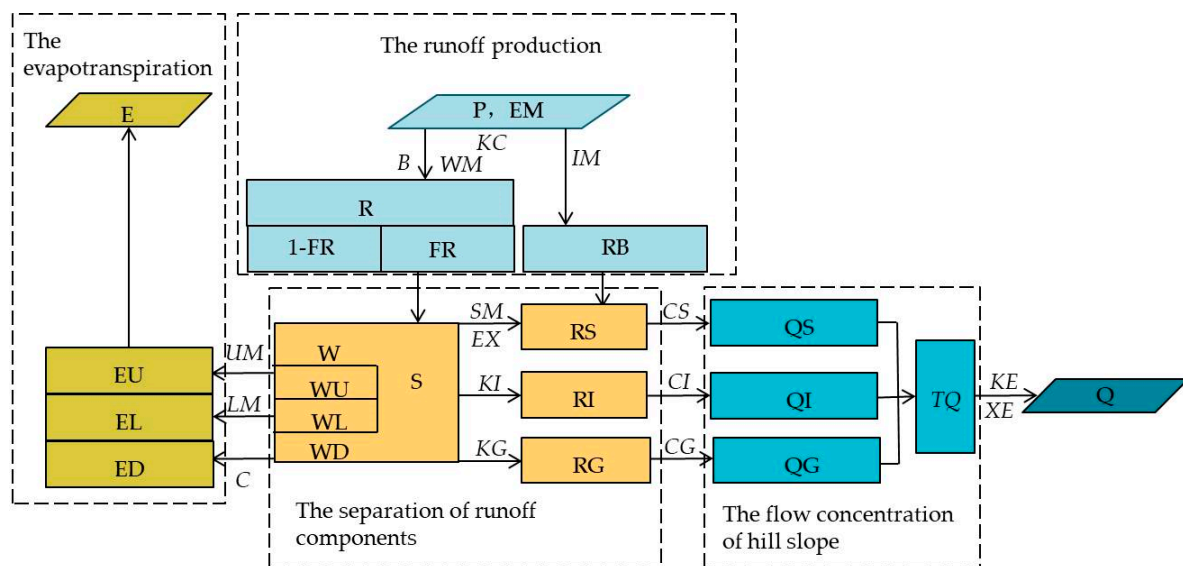| Symbol	Classify	Physical Meaning	Units	Range
KC		The ratio of potential evapotranspiration to pan evaporation	-	0.6–1.5
UM	Calculation for evapotranspiration	Tension water capacity of upper layer	mm	5–20
LM		Tension water capacity of lower layer	mm	60–90
C		The coefficient of deep evapotranspiration	-	0.08–0.18
WM	Calculation for runoff producing	Areal mean tension water capacity	mm	100–220
B		The exponent of the tension water capacity curve	-	0.1–0.4
SM		Free water storage capacity	mm	10–50
EX		The exponent of the free water capacity curve	-	1–1.5
KG	Calculation for separating water resources	Outflow coefficient of free water storage to the groundwater flow	-	0.2–0.6
KI		Outflow coefficient of free water storage to the interflow	-	0.2–0.6
CS		Recession constant of surface water storage	-	0.4–0.7
CI		Recession constant of interflow storage	-	0–0.9
CG	Calculation for runoff concentration	Recession constant of groundwater storage	-	0.98–0.998
KE		Residence time of water	h	0.5–1.5
XE		Muskingum coefficient	-	0–0.5

Figure 4. The structure of Xinanjiang Model.

Table 4. State variables in Xinanjiang model.

Symbol	Classify	Physical Meaning	Units
EM	Input	Pan evaporation of water surface	mm
E		Total evaporation	mm
EU	Calculation for	Evaporation in upper soil layer	mm
EL	evapotranspiration	Evaporation in lower soil layer	mm
ED		Evaporation in deep soil layer	mm
FR	Calculation for runoff	Fraction of runoff production area	-
IM	producing	Fraction of impervious area	-
RB		Runoff on impervious area	mm
W		Total tension water storage	mm
WU		Tension water storage in upper soil layer	mm
WL		Tension water storage in lower soil layer	mm
WD	Calculation for	Tension water storage in deep soil layer	mm
S	separating water	Free water storage capacity in upper soil layer	mm
RS	resources	Surface runoff	mm
RI		Interflow runoff	mm
RG		Groundwater runoff	mm
QS		Surface discharge	m^3/s
QI	Calculation for runoff	Interflow discharge	m^3/s
QG	concentration	Groundwater discharge	m^3/s
TQ		Total sub-basin inflow to the channel network	m^3/s
Q	Output	Basin discharge	m^3/s

Zhao et al. introduced a detailed method of parameter calibration [43]. The 15 parameters can be divided into four categories: evapotranspiration parameters (*KC*, *UM*, *LM*, and *C*), runoff producing parameters (*WM* and *B*), water resources separating parameters (*SM*, *EX*, *KG*, and *KI*) and runoff concentration parameters (*CS*, *CI*, *CG*, *KE*, and *XE*). Each category is basically independent from the others. Nine of these parameters (*KC*, *SM*, *KI*, *KG*, *CS*, *CI*, *CG*, *KE* and *XE*) are sensitive. The remaining ones are insensitive. The values of insensitive parameters are given according to the basin information. The data series are separated into calibration and validation periods. The calibration process is for the sensitive ones and is conducted according to the order of parameter category shown in Table 3.

When calibrating the parameters, the model is divided into daily model and hourly model. The input data of daily model are in daily intervals. It mainly aims at water balance and calibrates the parameters *KC*, *UM*, *LM*, *C*, *WM*, and *B*. The input data of hourly model are in hourly intervals. It calibrates the remaining parameters.

The goodness-of-fit measures used in the hourly model are relative error and certainty coefficient. The relative error contained the runoff depth and flood peek discharge.

$$ER = (Rsim - Robs)/Robs \qquad (10)$$

$$EQ = (Qm_{sim} - Qm_{obs})/Qmobs \qquad (11)$$

where *Robs* is observed runoff depth (mm), *Rsim* is calculated runoff depth (mm), Qm_{obs} is observed peak discharge (m^3/s), Qm_{sim} is calculated peak discharge (m^3/s), and *ER* and *EQ* are, respectively, related to runoff depth and peak discharge.

The certainty coefficient as follows:

$$DC = 1 - \sum_{i=1}^{n} (y_{ci} - y_{oi})^2 / \sum_{i=1}^{n} (y_{oi} - \overline{y_o})^2 \qquad (12)$$

where *DC* is the certainty coefficient, y_c is the simulative value, y_o is the observed value, $\overline{y_o}$ is the average of the observed value, and *n* is the length of data series.

3.2. Hydrology Data

3.2.1. Daily Model

There is no evaporation station in Dapoling basin. We used the data from evaporation station named Xinyang of Xixian basin. The Dapoling basin is a sub-basin of Xixian basin. The distance of Dapoling to Xinyang is about 60 km. We used the observed daily precipitation data from 13 rainfall stations daily evapotranspiration data of Xinyang station between 1965 and 2012 for the input of daily model. The daily discharge data of Dapoling station were used for parameter calibration.

3.2.2. Hourly Model

We selected 37 flood events (Table 5) between 1965 and 2012 in the Dapoling basin. The small flood events between 1965 and 2012 were not considered for calibrating the flood forecast system used by the basin management agency. Therefore, we chose the flood events that were larger than 900 m^3/s. To calculate the centroid of precipitation and runoff, we chose 28 single peak floods for lag time calculation.

Table 5. The flood events in Dapoling basin.

Flood Code	Calibration/Validation	Start Time	End Time	P	R	Qm
31650708	Calibration	08/07/1965 17:00	13/07/1965 6:00	146.7	179.3	2720
31650713 *	Calibration	13/07/1965 09:00	20/07/1965 8:00	79.2	68.3	1680
31650721 *	Calibration	21/07/1965 6:00	31/07/1965 7:00	143.6	114.4	2260
31650803 *	Calibration	03/08/1965 15:00	09/08/1965 7:00	73.7	97.4	1630
31670703 *	Calibration	03/07/1967 12:00	09/07/1967 20:00	174.3	112.6	3080
31680712	Calibration	12/07/1968 12:00	30/07/1968 17:00	4.6	342.7	3680
31690422 *	Calibration	22/04/1969 21:00	30/04/1969 16:00	91.4	72.6	1450
31710701 *	Calibration	01/07/1971 1:00	05/07/1971 22:00	84.5	71.0	1810
31720619	Calibration	19/06/1972 8:00	24/06/1972 20:00	2.1	54.1	916
31730429 *	Calibration	29/04/1973 11:00	03/05/1973 8:00	168.5	102.8	2110
31750805 *	Calibration	05/08/1975 2:00	13/08/1975 3:00	354.5	314.4	4220
31770708 *	Calibration	08/07/1977 18:00	14/07/1977 16:00	146.1	60.4	1100
31780624 *	Calibration	24/06/1978 8:00	30/06/1978 6:00	222.1	87.6	1510
31790911	Calibration	11/09/1979 8:00	19/09/1979 8:00	167.7	101.5	984
31800623 *	Calibration	23/06/1980 9:00	26/06/1980 15:00	170.1	103.1	1880
31810822 *	Calibration	22/08/1981 21:00	26/08/1981 4:00	163.2	88.9	2020
31820811 *	validation	11/08/1982 10:00	16/08/1982 19:00	136.4	107.6	1140
31840612 *	validation	12/06/1984 12:00	18/06/1984 7:00	131.9	68.5	1600
31870605 *	validation	05/06/1987 20:00	12/06/1987 7:00	124.4	75.2	1660
31890606 *	Calibration	06/06/1989 18:00	12/06/1989 7:00	260.2	152.3	3280
31890806	Calibration	06/08/1989 14:00	16/08/1989 8:00	208.9	211.7	2460
31910612	Calibration	12/06/1991 12:00	29/06/1991 16:00	199	119.6	1420
31910706 *	Calibration	06/07/1991 1:00	21/07/1991 8:00	121.1	79.3	1540
31910801 *	Calibration	01/08/1991 0:00	23/08/1991 16:00	227.6	124.9	1540
31960628 *	Calibration	28/06/1996 9:00	03/07/1996 8:00	164.2	51.1	1550
31970716 *	Calibration	16/07/1997 23:00	25/07/1997 16:00	106.6	48.9	1220
31980701 *	Calibration	01/07/1998 22:00	09/07/1998 8:00	88.9	68.8	1140
31980803 *	Calibration	03/08/1998 2:00	20/08/1998 16:00	492.7	340.4	1730
31030717 *	Calibration	17/07/2003 1:00	29/07/2003 0:00	159.6	72.9	1070
31050625 *	Calibration	25/06/2005 18:00	05/07/2005 0:00	159.6	73	1920
31050709*	Calibration	09/07/2005 2:00	12/07/2005 0:00	193.5	139.2	3520
31050829 *	Calibration	29/08/2005 2:00	05/09/2005 16:00	169.4	111.6	2580
31070703	Calibration	03/07/2007 0:00	06/07/2007 21:00	130.4	68.4	1370
31070707	Calibration	07/07/2007 0:00	12/07/2007 16:00	125.9	78.4	1040
31090828 *	validation	28/08/2009 13:00	07/09/2009 20:00	133.4	68.5	1140
31100715	validation	15/07/2010 8:00	21/07/2010 20:00	231.9	129	2020
31120907 *	validation	07/09/2012 0:00	10/09/2012 20:00	155.4	37.8	966

P refers to the observed rainfall, mm. *R* refers to the observed runoff depth, mm. *Qm* refers to the observed discharge, m^3/s. The flood code with "*" was used for lag time calculation.

The observed precipitation data for model input were from the 13 rainfall stations listed in Table 1. The data were converted to average rainfall data by the Thiessen polygon method to represent the basin rainfall to be used conveniently in the calculation of lag time. The observed discharge data were from the Dapoling station. Initial precipitation and discharge data were recorded every half hour, every hour, every two hours, every four hours, or another time interval. The time interval depended on the measure level of the stations during 1965 and 2012. The rainfall and discharge data were calculated into the hourly interval data. The observed evaporation data were from Xinyang station outside the basin. Initial evaporation data were recorded every day. The data were calculated into the hourly interval by arithmetic mean method. The whole period was divided into two periods of 1965−1985 and 1986−2012 according to Qu et al. [38] and Zhang et al. [39].

3.3. Data Processing

3.3.1. The Composing of Runoff Series

There are three test methods in the previous studies: the variation of the model errors of the whole period, the comparison of parameters in different periods, and the model simulation change compared with the reference period. One of the steps to test the change of data series is to run the model for some periods and compare the simulated runoff. In this study, the daily precipitation of rainfall stations and the daily evaporation were the input data for the model. The daily discharge was simulated by parameters of different periods. The authors found that the land use changed after 1985. Thus, the study period was divided into two parts of 1965−1985 and 1986−2012, according to the land use change tested in the previous study.

We set two scenarios: Scenario A represented the condition before land use change (1965–1985), and Scenario B represented the condition after change (1986–2012). The hydrologic data were divided into two parts according to the two scenarios.

Xinanjiang Model was used to calibrate parameters for the two parts separately and arrived at two sets of parameters. There were 18 flood events before 1985, of which 15 were for calibration and 3 for validation. There were 19 flood events after 1985, of which 16 were for calibration and 3 for validation. The set of parameters before land use change was named Parameter A, and the other was named Parameter B. Therefore, Parameter A represented the condition before land use change, and Parameter B represented after land use change.

When simulating runoff, we used Parameter A to simulate the runoff of 1986 and 2012. The inputs were the precipitation and evapotranspiration data of 1986 and 2012. The output discharge and the observed discharge of 1965 and 1985 composed the whole period discharge and named Series A. Parameter B was used to simulate the runoff of 1965 and 1985. The inputs were the precipitation and evapotranspiration data of 1965 and 1985. The output discharge and the observed discharge of 1986 and 2012 composed the whole period discharge named Series B. The data processing is shown in Figure 5. Therefore, the two-discharge series were both based on the same precipitation and evapotranspiration data, thus Series A represented Scenario A, and Series B represented Scenario B. The difference of the two-runoff series was only caused by the land use change.
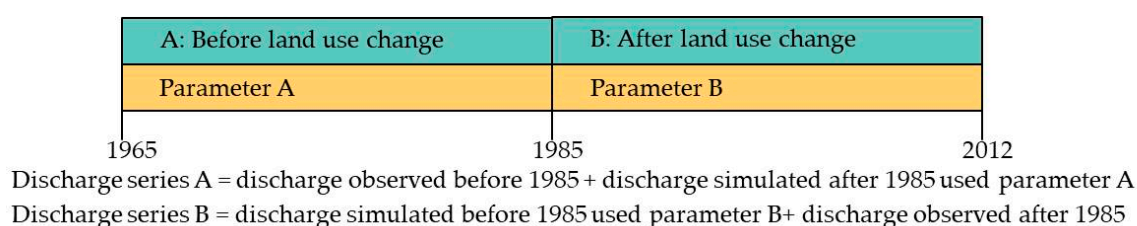

Discharge series A = discharge observed before 1985 + discharge simulated after 1985 used parameter A
Discharge series B = discharge simulated before 1985 used parameter B+ discharge observed after 1985

Figure 5. The data processing.

The comparison of runoff depth, flood peak, kurtosis coefficient, rainfall–runoff relationship and lag time was based on the two series. The lag time was calculated by the 28 single peak flood events. The others were calculated by all the flood events that participated in parameter calibration.

3.3.2. The Calculation of Lag Time

Four types of lag time are introduced in Figure 6 [23]: T_{LPC} is the centroid lag-to-peak time from the centroid of precipitation to the peak discharge; T_{LC} is the centroid lag time from the centroid of precipitation to the centroid of discharge; T_{LP} is the lag-to-peak time from the beginning of precipitation to the peak discharge; and T_{LPP} is the peak lag-to-peak time from the peak rainfall intensity to the peak discharge. The centroid lag time T_{LC} equals to the mean flow concentration time of the basin that is usually meant.
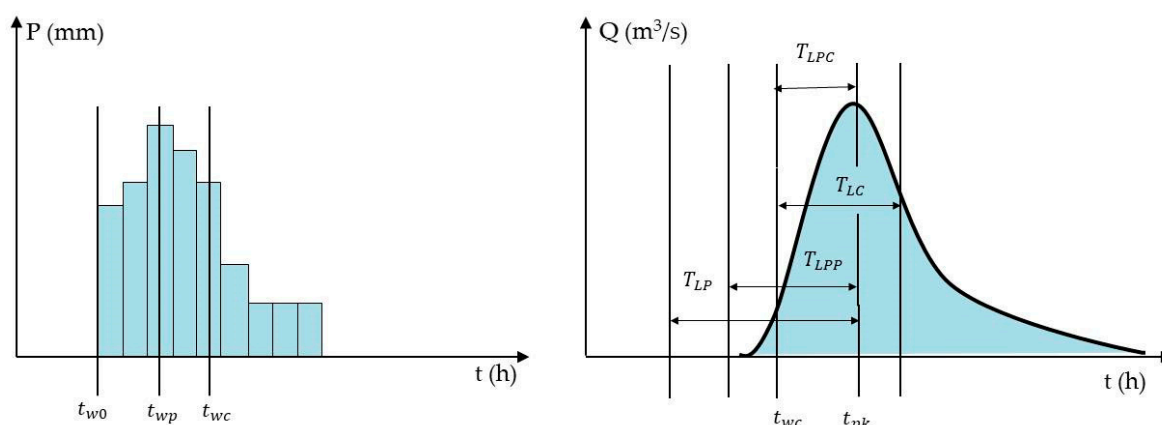

Figure 6. Definitions of terms used to describe hyetographs and response hydrographs. t_{w0}, beginning of precipitation; t_{wp}, peak of precipitation; t_{wc}, centroid of precipitation; t_{pk}, time of peak discharge; t_{qc}, centroid of runoff; T_{LPC}, centroid lag-to-peak; T_{LC}, centroid lag; T_{LP}, lag-to-peak; T_{LPP}, peak lag-to-peak. The other variables are the same as above.

The four types of lag time represent the time index of the runoff produced by the precipitation. The centroid lag time T_{LC} equals the basin mean concentration time, therefore the information of concentration time can be obtained from the calculation of T_{LC}. The other three lag times are all relative with the time of peak discharge.

The centroid of precipitation was determined by:

$$t_{wc} = \sum_{i=1}^{n} w_i \times t_i / \sum_{i=1}^{n} w_I \tag{13}$$

where t_{wc} is centroid of precipitation, w_i is precipitation for period i, t_i is time for period i, and n is the data size. The centroid of runoff was determined by:

$$t_{qc} = \sum_{i=1}^{n} Q_i \times t_i / \sum_{i=1}^{n} I \tag{14}$$

where t_{qc} is centroid of runoff, Q_i is mean runoff for period i.

The runoff depth, flood peak and kurtosis coefficient were calculated for all the selected floods. The runoff depth was determined by:

$$R = 3.6Q\Delta t/F \tag{15}$$

where R is runoff depth (mm), Q is mean discharge (m^3/s), Δt is time interval (h), and F is area for the basin (km^2). The average value was determined by:

$$\text{average} = \frac{\sum_{i=1}^{n} x_i}{n} \tag{16}$$

The mean square error was determined by:

$$s = \sqrt{\frac{1}{n} \sum_{i=1}^{n} (x_i - \bar{x})^2} \tag{17}$$

where s is mean square error, x_i is variable value, and $\bar{x}$ is mean variable value. The kurtosis coefficient k was determined by:

$$k = \Sigma_{i=1}^{n} (x_i - \bar{x})^4 / \left[(n-1)s^4 \right] \tag{18}$$

The variables in Equation (18) have the same meaning as before.

3.3.3. The Calculation of Rainfall–Runoff Relationship

The rainfall–runoff correlogram reflects the quantitative relationship between one rainfall event and the total amount of corresponding flood. This research adopted the Antecedent Precipitation Index (Pa) to study the rainfall–runoff relationship in Dapoling basin. The linear regression equation was used to simulate the relationship between rainfall and runoff:

$$y = ax + b \tag{19}$$

where y is runoff depth (R/mm) and x is the sum of precipitation (P/mm) and its antecedent precipitation index (Pa/mm). The values of x and y were calculated for every event.

The slope of the line "a" reflects the runoff efficiency, and the x-intercept "b" reflects the rainfall threshold that produces runoff.

4. Results and Discussion

4.1. Parameters Change of the Basin

The parameters before/after land use change are shown in Tables 6 and 7. The results in Table 7 show that the relative errors of runoff depth and peak discharge were all less than 0.25, and the certainty coefficients were all larger than 0.78. Twenty-eight of the 37 flood events qualified the inspection standard. The simulative result is good.

Table 6. Parameters of the two periods before/after land use change.

Parameters	Periods	
	1965−1985	1986−2009
KC	0.77	0.95
WM (mm)	150	145
UM (mm)	20	20
LM (mm)	80	80
B	0.3	0.27
C	0.167	0.167
SM (mm)	13	13
EX	1.5	1.5
KI	0.42	0.50
KG	0.28	0.20
CS	0.55	0.56
CI	0.85	0.90
CG	0.993	0.994
KE (h)	1.4	1.2
XE	0.18	0.20

Table 7. The simulation results of Xinanjiang Model in Dapoling Basin.

Periods	Flood Code	R_{sim} (mm)	R_{obs} (mm)	ER	Qm_{sim} (m³/s)	Qm_{obs} (m³/s)	EQ	DC
1964–1985	31650708	152.2	179.3	0.151	3057	2720	−0.124	0.898
	31650713	58.1	68.3	0.149	1508	1680	0.102	0.97
	31650721	121.9	114.4	−0.066	2011	2260	0.110	0.899
	31650803	75.2	97.4	0.228	1252	1630	0.232	0.816
	31670703	127.5	112.6	−0.132	3311	3080	−0.075	0.878
	31680712	361.4	342.7	−0.055	3360	3680	0.087	0.984
	31690422	90.4	72.6	−0.245	1143	1450	0.212	0.783
	31710701	79.8	71	−0.124	1659	1810	0.083	0.896
	31720619	65.5	54.1	−0.211	938	916	−0.024	0.895
	31730429	116	102.8	−0.128	1768	2110	0.162	0.864
	31750805	313.4	314.4	0.003	3837	4220	0.091	0.96
	31770708	70.2	60.4	−0.162	1258	1100	−0.144	0.938
	31780624	109.6	87.6	−0.251	1606	1510	−0.064	0.952
	31790911	114.7	101.5	−0.130	979	984	0.005	0.862
	31800623	101.7	103.1	0.014	1736	1880	0.077	0.978
	31810822	100.7	88.9	−0.133	1812	2020	0.103	0.922
	31820811	106.7	107.6	0.008	1221	1140	−0.071	0.842
	31840612	68.5	68.5	0.000	1372	1600	0.143	0.973
1986–2012	31870605	79	75.2	−0.051	1580	1660	0.048	0.982
	31890606	138.7	152.3	0.089	3054	3280	0.069	0.911
	31890806	153.8	211.7	0.274	2716	2460	−0.104	0.665
	31910612	119	119.6	0.005	1240	1420	0.127	0.957
	31910706	76	79.3	0.042	1467	1540	0.047	0.968
	31910801	129.9	124.9	−0.040	1655	1540	−0.075	0.982
	31960628	63.2	51.1	−0.237	1415	1550	0.087	0.863
	31970716	53.1	48.9	−0.086	1237	1220	−0.014	0.968
	31980701	68.7	68.8	0.001	1173	1140	−0.029	0.895
	31980803	382.9	340.4	−0.125	1591	1730	0.080	0.89
	31030717	77.1	72.9	−0.058	988	1070	0.077	0.875
	31050625	66.9	73	0.084	1869	1920	0.027	0.994
	31050709	127.1	139.2	0.087	3237	3520	0.080	0.979
	31050829	111.7	111.6	−0.001	2105	2580	0.184	0.903
	31070703	77.5	68.4	−0.133	1117	1370	0.185	0.373
	31070707	86.4	78.4	−0.102	912	1040	0.123	-0.356
	31090828	81.7	68.5	−0.193	1190	1140	−0.044	0.888
	31100715	122.4	129	0.051	2046	2020	−0.013	0.928
	31120907	49.2	37.8	−0.302	990	966	−0.025	0.545

Robs is observed runoff depth; *Rsim* is calculated runoff depth; *Qm_obs* is observed peak discharge; *Qm_sim* is calculated peak discharge, *ER* and *EQ* are related to runoff depth and peak discharge, respectively; *DC* is certainty coefficient.

The results in Table 6 show that the parameters of Xinanjiang Model varied largely after land use change, especially the sensitive ones. The ratio of potential evapotranspiration to pan evaporation *KC* enlarged from 0.77 to 0.95 after land use change, which means that the existing land use type promotes more evapotranspiration than runoff losses. The areal mean tension water capacity *WM* decreased from 150 to 145 mm. The three recession constants (surface water storage *CS*: 0.55–0.56; interflow storage *CI*: 0.85–0.9; and groundwater storage *CG*: 0.993–0.994) increased after land use change, which means that the runoff would recess slowly. The outflow coefficient of free water storage to the interflow *KI* (0.42–0.5) increased, and the outflow coefficient of free water storage to the groundwater flow *KG* (0.28–0.2) decreased after land use change. The land use data (Table 2 and Figure 2) show that, after 1985, the area of water and paddy field increased. The increase might have caused the above variation of runoff recession.

4.2. Runoff Depth

The calculated results of runoff depth before and after land use change in the basin are shown in Tables 8 and 9. The results in Table 8 indicate that the mean runoff depth after land use change (Series B) was slightly larger than that before land use change (Series A). The land use data in Table 2 express that the general variation trend of woodland and farmland decreased, while the urban land increased. This might have caused the slight increase of runoff depth. For the aspect of parameters of Xinanjiang Model in Table 3, the evaporation coefficient *KC* increased after land use change, indicating more consumption of water, while the areal mean tension water capacity *WM* reduced after land use change, indicating more production of water, which means that perhaps the *WM* influenced more. In addition, the mean square error after land use change was larger than that before land use change (before: 49.90; after: 50.04). The land use data in Table 2 show that, after 1985, the water and the paddy field increased and the farmland decreased, which may reduce the infiltration and produce more water. Other research [16] shows that the decreasing of farmland may cause runoff reducing. In Dapoling basin, the farmland decreased slightly (from 41.85% to 41.81%), which might have some impact on the variation of runoff. This means that, if the land use of an area tends to vary similarly with this condition, the runoff of a flood may increase. This has meaningful guidance to flood management.

Table 8. The result of hydrologic variables in Dapoling basin.

Statistics	R		Q_m		Kr	
	Series A	Series B	Series A	Series B	Series A	Series B
Maximum	314.4	310.0	4220	3740	16.7	18.2
Minimum	39.9	37.7	892	966	2.4	2.2
Variation range	274.5	272.3	3328	2774	14.3	16.0
Average	87.16	92.49	1821	1916	7.50	7.66
s	49.90	50.04	795	774	3.70	3.99

R refers to runoff depth (mm), Q_m refers to flood peak (m³/s), *s* refers to mean square error, and the other variables are the same as above and below.

Table 9. The result of hydrologic variables of different rainfall in Dapoling basin.

Rainfall (mm)	Statistics	R		Q_m		Kr	
		Series A	Series B	Series A	Series B	Series A	Series B
<100 (7 events)	Maximum	97.4	103.1	1680	2210	16.7	18.2
	Minimum	45.6	48.9	1100	1070	3.6	4.2
	Average	66.1	70.0	1403	1440	9.6	9.3
100–200 (23 events)	Maximum	124.9	131.8	3630	3570	11.8	12.9
	Minimum	39.9	37.7	892	966	2.4	2.2
	Average	82.2	87.3	1838	1999	6.6	7.2
>200 (7 events)	Maximum	314.4	310.0	4220	3740	7.3	5.8
	Minimum	87.6	101.1	1510	1680	5.1	4.9
	Average	176.8	187.8	2980	2900	5.9	5.2

Among the range of rainfall exceeding 200 mm, five events were between 200 mm and 300 mm, one event was between 300 mm and 400 mm, and one event was greater than 400 mm. The same as below.

There were seven events with rainfall of less than 100 mm, 23 events with rainfall of between 100 mm and 200 mm, and seven events with rainfall of greater than 200 mm. Among the events with rainfall greater than 200 mm, five were between 200 mm and 300 mm, one was between 300 mm and 400 mm, and one was greater than 400 mm. Data in Table 9 indicate that the variation of runoff depth was influenced slightly by different size of rainfall events. The result for rainfall greater than 200 mm could not be obtained due to the lack of flood sample. This means that the result can only be implicated for the rainfall that smaller than 200 mm.

4.3. Flood Peak

The result of flood peak before and after land use change in Dapoling basin is shown in Tables 8 and 9. Table 8 indicates that the mean flood peak has increased due to land use change, which increased from 1821 m^3/s before land use change (Series A) to 1916 m^3/s after land use change (Series B). The maximum value of flood peak reduced after 1985 (from 4220 to 3740 m^3/s). Land use data in Table 2 show that, after 1985, the water and paddy field increased, which means that the regulation and storage of water might have reduced the flood peak.

Data in Table 9 show the relationship between the variation of flood peak before/after land use change and the precipitation level. The mean flood peak after land use change was larger than that before land use change when rainfall was less than 200 mm. The variation of mean flood peak when rainfall was greater than 200 mm additionally could not be obtained obviously due to the lack of flood sample. However, Hood et al. [23] indicated that the variation of flood peak is related with the size of the rainfall event in low impact and traditional residential development areas [23].

4.4. Kurtosis Coefficient

The kurtosis coefficient reflects the shape of discharge hydrograph to a certain degree. The larger the kurtosis is, the more leptokurtic the hydrograph is, which has more values around the mean than a normal distribution. Leptokurtic hydrograph means that the flood rises and recesses rapidly. The result of kurtosis coefficient before and after land use change in Dapoling basin is shown in Tables 8 and 9. It can be concluded that the kurtosis coefficient after land use change (Series B) was larger than that before land use change (Series A). A larger kurtosis coefficient means more leptokurtic distribution of discharge hydrograph, which indicates that the flood after land use change rises and recesses more rapidly than that before land use change. This may be related with the increasing of urban area (from 0.63 to 0.88).

4.5. Rainfall–Runoff Relationship

The rainfall–runoff correlograms before and after land use change are shown in Figure 7. The equation before land use change is as follows:
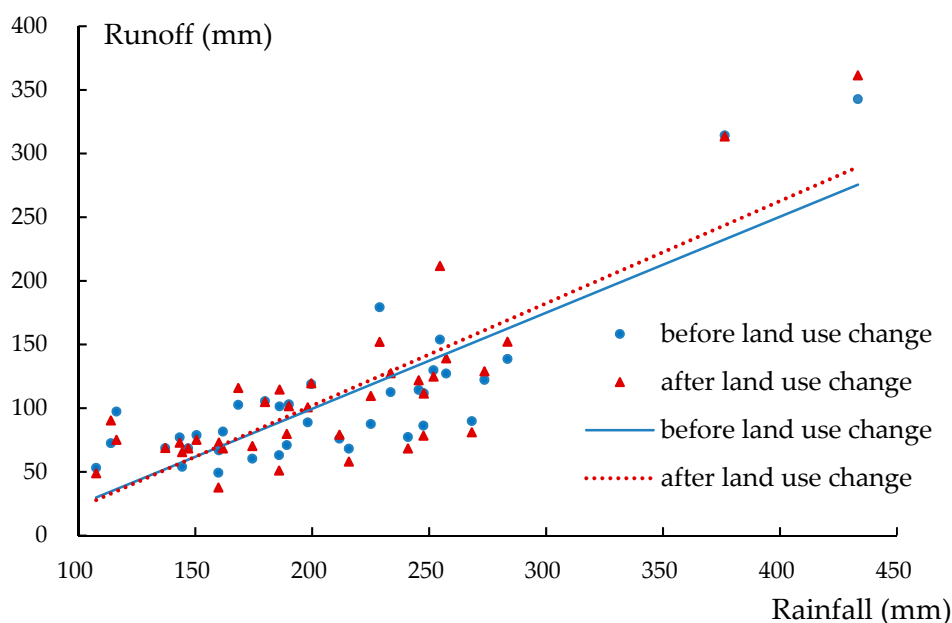
$$y = 0.7544x - 51.314 \tag{20}$$

Figure 7. The relationship between precipitation and runoff depth.

The equation after land use change is as follows:

$$y = 0.8033x - 58.623 \tag{21}$$

where y represents runoff depth (R/mm) of per event and x represents the sum of precipitation (P/mm) and its antecedent precipitation index (Pa/mm).

According to the result in Figure 7, the slope of the line after land use change was slightly larger than that before land use change, which means that the rainfall after land use change may produce more runoff than that before land use change. This is consistent with the change of runoff depth discussed above. The x-intercept after land use change was larger than that before land use change (Figure 7), which means that the rainfall after land use change produces runoff more difficult.

4.6. Mean Lag Time Change of the Basin

The results indicate that the mean basin lag time varied before/after 1985. The result of centroid lag-to-peak time T_{LPC} is shown in Table 10. Compared with Series A, the mean centroid lag-to-peak time T_{LPC} of Series B decreased from 11.92 h to 11.67 h. The mean square error has slightly increased from 9.97 to 10.21. The decreased T_{LPC} means that the flood peak after land use change may come faster than that before land use change. The centroid lag-to-peak time T_{LPC} in all selected floods is positive. Other studies found that the mean centroid lag-to-peak time T_{LPC} may be negative [23]. The negative values of the lag time are caused by the strong rainfall intensity occurring at the beginning of the precipitation. The intensity reaches its maximum soon after the precipitation. The long duration but low intensity precipitation process after the maximum leads to the centroid of precipitation towards right deviation, while the peak of the runoff appears soon after the peak rainfall intensity.

Table 10. The average values of mean basin lag times in the basin.

Statistics	T_{LPC}		T_{LC}		T_{LP}		T_{LPP}	
	Series A	Series B	Series A	Series B	Series A	Series B	Series A	Series B
Maximum	58.6	59.6	67.4	62.4	61	63	28	28
Minimum	2.9	1.5	6.6	6.9	10	10	4	4
Variation range	55.7	58.0	60.8	55.5	51.0	53.0	24.0	24.0
Average	11.92	11.67	25.28	25.10	17.00	22.57	11.11	10.86
s	9.97	10.21	11.01	11.73	11.51	11.68	4.69	4.86

T_{LPC} means centroid lag-to-peak, T_{LC} means centroid lag, T_{LP} means lag-to-peak, T_{LPP} means peak lag-to-peak, s means mean square error, the units in the table is h, the same as below.

Similarly, the calculated centroid lag time T_{LC} also varied before/after 1985. The results are shown in Table 10. In Table 10, the average T_{LC} slightly decreased from 25.28 h to 25.10 h. In addition, the variation range of centroid lag time T_{LC} after land use change was smaller. Before land use change, the T_{LC} varied from 6.6 h to 67.4 h, and its range was 60.8 h. The mean square error of T_{LC} of Series A was 11.01. After land use change, the T_{LC} varied from 6.9 h to 62.4 h, and its range was 55.5 h, with a mean square error of it was 11.73. T_{LC} is the centroid lag time from the centroid of precipitation to the centroid of discharge, which means that T_{LC} represents the mean concentration time of the basin. These variations of T_{LC} indicate that the land use change resulted in the mean concentration time variation of the basin. The decreased average T_{LC} means that the existing land use reduces the mean basin concentration time. The maximum value of T_{LC} is smaller after land use change, while the minimum value is larger than that before 1985. This means that, after land use change, the distribution of the flood concentration time is more intensive.

The calculated results of lag-to-peak time T_{LP} are shown in Table 10. The results indicate that the lag-to-peak time T_{LP} after land use change was different from that before land use change. The average value under the condition after land use change was 1.33 times that before land use change. This means that the flood peak comes slower after land use change. In addition, the variation range

of lag-to-peak time after land use change was larger than that before land use change. Before land use change, the T_{LP} varied from 10 h to 61 h, the range was 51 h and the mean square error was 11.51. After land use change, the T_{LP} varied from 10 h to 63 h, the range of which was 53 h and mean square error was 11.68. Lag-to-peak time T_{LP} was positively correlated with precipitation duration (r: Series A: 0.834; Series B: 0.847) and runoff depth (r: Series A: 0.627; Series B: 0.605) before/after land use change. No relation was found among centroid lag-to-peak time T_{LPC}, centroid lag time T_{LC} or peak lag-to-peak time T_{LPP} and precipitation duration or runoff depth (r < 0.35).

The calculated results of mean peak lag-to-peak time T_{LPP} are shown in Table 10. The results show that the peak lag-to-peak time T_{LPP} after land use change was slightly different from that before land use change. The average value after land use change was smaller than that before land use change (Series A: 11.11 h; Series B: 10.86 h), which means that the time of peak discharge will appear more quickly after land use change. In addition, the range of peak lag-to-peak time after land use change was similar to that before land use change. For the two series, the maximum value of T_{LPP} was 28 h, and the minimum value was 4 h, but the mean square errors were different (Series A: 4.69; Series B: 4.86). The variation of mean square error indicates that the distribution range of the time from peak precipitation to peak discharge was slightly wider.

The mean basin lag times in different rainfall are shown in Table 11. The results in Table 11 show that the change of mean basin lag time varies with different rainfall depth. When the rainfall depth was less than 100 mm, the four kinds of lag times increased after land use change. When the rainfall was between 100 mm and 200 mm, the four kinds of lag times of Series B decreased compared with Series A. When the rainfall was greater than 200 mm, the T_{LC} decreased, while the other three lag times seldom changed. Since the number of the events when rainfall was greater than 200 mm was few, the results of that condition need to be further studied.

Table 11. The lag times for different rainfall.

Rainfall (mm)	Statistics	T_{LPC}		T_{LC}		T_{LP}		T_{LPP}	
		Series A	Series B	Series A	Series B	Series A	Series B	Series A	Series B
<100 (7 events)	Maximum	15	16	41.4	47.4	39	35	15	14
	Minimum	2.9	2.5	19.6	11.7	13	13	4	6
	Average	8.65	9.10	25.79	26.73	20.33	20.78	9.44	9.89
100–200 (23 events)	Maximum	58.6	59.6	67.4	62.4	34	32	28	28
	Minimum	3.5	1.5	6.6	6.9	10	10	6	4
	Average	12.95	12.26	25.28	24.97	20.38	19.69	11.50	10.81
>200 (7 events)	Maximum	19.4	19.8	28.5	25.2	61	63	18	20
	Minimum	11.6	9.6	20.5	18.8	21	19	10	10
	Average	16.27	16.27	23.71	20.90	43.33	43.33	14.00	14.00

Synthesizing the results in Tables 10 and 11, different lag times were influenced by different size of rainfall events. The results in in Table 10 show that, for the all rainfall events, the values of centroid lag-to-peak time T_{LPC}, centroid lag time T_{LC} and peak lag-to-peak time T_{LPP} decreased after land use change. The results in Table 11 show that, when the rainfall was between 100 and 200 mm, the above three lag times decreased after land use change, while, for other rainfall events, the three lag times increased or changed slightly. Therefore, the centroid lag-to-peak time T_{LPC}, centroid lag time T_{LC} and peak lag-to-peak time T_{LPP} were influenced more by the rainfall events that were between 100 mm and 200 mm than other events. For the lag-to-peak time T_{LP}, the mean value of all the events increased after land use change (Table 10). However, the results in Table 11 reveal that, when the rainfall was less than 100 mm, the value of T_{LP} increased after land use change, which expressed that the T_{LP} was influenced more by the rainfall events smaller than 100 mm.

This study compared the variation of four types of lag time before and after land use change in Dapoling basin by calculating the selected 28 flood events based on Xinanjiang Model. In the management of basin flood forecasting, different precipitation processes arrive at the time of peak discharge. Once the mean concentration time was determined, T_{LP}, T_{LPP} and T_{LPC} could be reached

from the time that the precipitation begins, the peak of precipitation appears and the precipitation ends in the whole process of precipitation. During the process of floods, the beginning time of precipitation is the most easily obtained. It is obvious that, if we want to obtain the time of peak discharge as early as possible, T_{LP} is the most useful information, because we only need to know the beginning time of precipitation. The uncertainty of the future precipitation makes it hard to judge the peak of rainfall, thus the information of T_{LPP} is difficult use. If the rainstorm center is in the upstream far away from the downstream, and the peak discharge does not appear in the downstream after the whole rainfall process, the time of peak discharge in the downstream can be obtained from T_{LPC}. Every type of lag time has its characteristics, which means that it is necessary to choose appropriate types according to actual situation in basin flood management. The determination of average log time of a basin makes flood forecasting easier. When a flood event comes, the time of flood peak could be predicted.

The variation of the mean basin lag times for two periods was due to the land use change. Data in Table 2 indicate that land use types changed from the 1980s to the 1990s and form the 1990s to the 2000s. In addition, the fact that after 1985 the land use changed revealed by the variation of lag time distribution and the presence of outliers may relate with the land use data, which is a future aspect of this study.

5. Conclusions

Considering land use change, this study used the Xinanjiang Model to calibrate parameters before/after land use change and to compare the hydrology response to the change. The research showed that the parameters varied after the change. The change of parameters means that the existing land use promotes more evapotranspiration and consumes more water. The runoff discharge will recess more slowly. This may increase the difficulty of travel and rescue in the future. It is meaningful for the government to make contingency plans for the floods in this region.

Additionally, the variation results of the runoff depth, flood peak and kurtosis coefficient relationship showed that they have increased slightly after land use change for floods produced by rainfall smaller than 200 mm. The analysis of rainfall–runoff relationship revealed that the rainfall after land use change produced more runoff with less production threshold. Refering to the land use data, we found that the change of water, paddy field and farmland may be the main land uses that influence the change of these hydrology elements.

Due to the lack of huge floods, the variation of runoff depth, flood peak and kurtosis coefficient for floods produced by rainfall greater than 200 mm could not be well obtained. More flood events data should be collected to obtain a more useful conclusion. Dapoling basin is the head source of Huai River basin. There are some basins with similar environment in Huai River basin. The parameters of Dapoling can be the reference of other basins when calibrating hydrology model and the results obtained in Dapoling basin can be extended to other sub-basins in the Huai River basin, which can provide important references for soil and water conservation, water resources use and management of land use in the Huai River.

Author Contributions: Conceptualization, M.Z. and S.Q.; Methodology, M.Z. and S.Q.; Software, M.Z. and S.X.; Validation, X.C. and H.Z.; Formal Analysis, M.Z.; Investigation, M.Z.; Resources, S.Q. and H.C.; Data Curation, J.G.; Writing—Original Draft Preparation, M.Z.; Writing—Review and Editing, P.S. and X.C.; Visualization, M.Z.; Supervision, S.Q.; Project Administration, P.S.; and Funding Acquisition, S.Q. and P.S.

References

1. Potter, K.W. Hydrological impacts of changing land management practices in a moderate-sized agricultural catchment. *Water Resour. Res.* **1991**, *27*, 845–855. [CrossRef]

2. Vörösmarty, C.J.; Green, P.; Salisbury, J.; Lammers, R. Global water resources: Vulnerability from climate change and population growth. *Science* **2000**, *289*, 284–288. [CrossRef]

3. Wan, R.; Yang, G. Progress in the Hydrological Impact and Flood Response of Watershed Land Use and Land Cover Change. *J. Lake Sci.* **2004**, *16*, 258–264. [CrossRef]

4. Yang, T.; Zhang, Q.; Wang, W.; Yu, Z.; Chen, Y.D.; Lu, G.; Hao, Z.; Baron, A.; Zhao, C.; Chen, X.; et al. Review of Advances in Hydrologic Science in China in the Last Decades: Impact Study of Climate Change and Human Activities. *J. Hydrol. Eng.* **2013**, *18*, 1380–1384. [CrossRef]

5. Calder, I.R.; Maidment, D.R. *Maidment D. R. Handbook of Hydrology*; McGraw-Hill: NewYork, NY, USA, 1993; Volume 13.

6. Guo, Z.; Ma, Y.; Li, H.; Liu, W. Effect of Land Use Change on Runoff in the Liushahe Watershed, Xishuangbanna Southwest China. *Res. Soil Water Conserv.* **2006**, *13*, 139–142. [CrossRef]

7. Yuan, F.; Ren, L.L.; Chen, X.; Chen, Y.D.; Xia, J.; Zhang, H. Evaluating the influence of land-cover change on catchment hydrology through the modified Xinanjiang model. In Proceedings of the International Association of Hydrological Sciences & the International Water Resources Association Conference, Guangzhou, China, 8–10 June 2006; pp. 167–174.

8. Li, K.Y.; Coe, M.T.; Ramankutty, N.; Jong, R.D. Modeling the hydrological impact of land-use change in West Africa. *J. Hydrol.* **2007**, *337*, 258–268. [CrossRef]

9. Liu, M.; Tian, H.; Chen, G.; Ren, W.; Zhang, C.; Liu, J. Effects of Land-Use and Land-Cover Change on Evapotranspiration and Water Yield in China During 1900-2000[1]. *J. Am. Water Resour. Assoc.* **2010**, *44*, 1193–1207. [CrossRef]

10. Yan, H.; Edwards, F.G. Effects of Land Use Change on Hydrologic Response at a Watershed Scale, Arkansas. *J. Hydrol. Eng.* **2013**, *18*, 1779–1785. [CrossRef]

11. Zhang, H.; Huang, Q.; Zhang, Q.; Gu, L.; Chen, K.; Yu, Q. Changes in the long-term hydrological regimes and the impacts of human activities in the main Wei River, China. *Hydrol. Sci. J.* **2016**, *61*, 1054–1068. [CrossRef]

12. Costa, M.H.; Botta, A.; Cardille, J.A. Effects of large-scale changes in land cover on the discharge of the Tocantins River, Southeastern Amazonia. *J. Hydrol.* **2003**, *283*, 206–217. [CrossRef]

13. Wang, G.; Zhang, Y.; Liu, G.; Chen, L. Impact of land-use change on hydrological processes in the Maying River basin, China. *Sci. China Ser. D Earth Sci.* **2006**, *49*, 1098–1110. [CrossRef]

14. Nazarnejad, H.; Solaimani, K.; Shahedi, K.; Sheikh, V. Evaluating hydrological response to land use change using the AGWA-GIS based hydrologic modeling tools. *Int. J. Agric. Res. Rev.* **2012**, *2*, 942–948. [CrossRef]

15. Vanshaar, J.R.; Haddeland, I.; Lettenmaier, D.P. Effects of land-cover changes on the hydrological response of interior Columbia River basin forested catchments. *Hydrol. Process.* **2002**, *16*, 2499–2520. [CrossRef]

16. Shi, P.; Zhang, Y.; Ren, Z.; Yu, Y.; Li, P.; Gong, J. Land-use changes and check dams reducing runoff and sediment yield on the Loess Plateau of China. *Sci. Total Environ.* **2019**, *664*, 984–994. [CrossRef]

17. Keesstra, S.D.; Davis, J.; Masselink, R.H.; Casalí, J.; Peeters, E.T.; Dijksma, R. Coupling hysteresis analysis with sediment and hydrological connectivity in three agricultural catchments in Navarre, Spain. *J. Soils Sediments* **2019**, *19*, 1598–1612. [CrossRef]

18. Abdulkareem, J.H.; Pradhan, B.; Sulaiman, W.N.A.; Jamil, N.R. Long-term runoff dynamics assessment measured through land use/cover (LULC) changes in a tropical complex catchment. *Environ. Syst. Decis.* **2019**, *39*, 16–33. [CrossRef]

19. Brath, A.; Montanari, A.; Moretti, G. Assessing the effect on flood frequency of land use change via hydrological simulation (with uncertainty). *J. Hydrol.* **2006**, *324*, 141–153. [CrossRef]

20. Fohrer, N.; Haverkamp, S.; Eckhardt, K.; Frede, H.-G. Hydrologic Response to land use changes on the catchment scale. *Phys. Chem. Earth Part B Hydrol. Oceans Atmos.* **2001**, *26*, 577–582. [CrossRef]

21. De Roo, A.; Odijk, M.; Schmuck, G.; Koster, E.; Lucieer, A. Assessing the effects of land use changes on floods in the Meuse and Oder catchment. *Phys. Chem. Earth Part B Hydrol. Oceans Atmos.* **2001**, *26*, 593–599. [CrossRef]

22. Mao, D.; Cherkauer, K.A. Impacts of land-use change on hydrologic responses in the Great Lakes region. *J. Hydrol.* **2009**, *374*, 71–82. [CrossRef]

23. Hood, M.J.; Clausen, J.C.; Warner, G.S. Comparison of Stormwater Lag Times for Low Impact and Traditional Residential Development1. *J. Am. Water Resour. Assoc.* **2010**, *43*, 1036–1046. [CrossRef]

24. Leopold, L.B. Lag times for small drainage basins. *Catena* **1991**, *18*, 157–171. [CrossRef]

25. Watt, W.E.; Chow, K.C.A. A general expression for basin lag time. *Can. J. Civ. Eng.* **1985**, *12*, 294–300. [CrossRef]

26. Loukas, A.; Quick, M. Physically-based estimation of lag time for forested mountainous watersheds. *Int. Assoc. Sci. Hydrol. Bull.* **1996**, *41*, 1–19. [CrossRef]

27. Elsenbeer, H.; Vertessy, R.A. Stormflow generation and flowpath characteristics in an Amazonian rainforest catchment. *Hydrol. Process.* **2015**, *14*, 2367–2381. [CrossRef]

28. Kang, I.S.; Park, J.I.; Singh, V.P. Effect of urbanization on runoff characteristics of the On-Cheon Stream watershed in Pusan, Korea. *Hydrol. Process.* **2015**, *12*, 351–363. [CrossRef]

29. Talei, A.; Chua, L.H.C.; Quek, C. A novel application of a neuro-fuzzy computational technique in event-based rainfall-runoff modeling. *Expert Syst. Appl.* **2010**, *37*, 7456–7468. [CrossRef]

30. Talei, A.; Chua, L.H.C. Influence of lag time on event-based rainfall–runoff modeling using the data driven approach. *J. Hydrol.* **2012**, *438–439*, 223–233. [CrossRef]

31. Li, M.; Li, Q.; Cai, T.; Li, P.; Zou, Z. Modeling the effects of land-use change on runoff generation in the upper Huaihe River basin, China. In Proceedings of the 2012 International Symposium on Geomatics for Integrated Water Resource Management, Lanzhou, China, 19–21 October 2012; pp. 1–4.

32. Chen, J.; Yu, Z.; Zhu, Y.; Yang, C. Relationship Between Land Use and Evapotranspiration-A Case Study of the Wudaogou Area in Huaihe River basin. *Procedia Environ. Sci.* **2011**, *10*, 491–498. [CrossRef]

33. Li, Q.; Cai, T.; Yu, M.; Lu, G.; Xie, W.; Bai, X. Investigation into the impacts of land-use change on sediment yield characteristics in the upper Huaihe River basin, China. *J. Hydrol. Eng.* **2013**, *18*, 1464–1470. [CrossRef]

34. Wen, H.; Li, Q.; Li, P.; Cai, T. Analysis of Impact of Land Use Change on Runoff Characteristics. *Water Resour. Power* **2013**, *31*, 12–14.

35. Dong, J.; Chen, Q. Study on Relationship between Land Use Changes and Surface Water Quality in Western Regions of Xinyang City. *Water Resour. Power* **2010**, *5*, 29–32.

36. Yu, L.; Xia, Z.; Li, Q.; Cai, T.; Guo, L.; Xie, W. Analysis of impact of land utilization change on non-point source pollution. *Water Resour. Power* **2012**, *30*, 100–102.

37. Cai, T.; Li, Q.; Yu, M.; Lu, G.; Cheng, L.; Wei, X. Investigation into the impacts of land-use change on sediment yield characteristics in the upper Huaihe River basin, China. *Phys. Chem. Earth Part B Hydrol. Oceans Atmos.* **2012**, *53–54*, 1–9. [CrossRef]

38. Qu, S.; Bao, W.; Shi, P.; Yu, Z.; Zhang, B. Evaluation of Runoff Responses to Land Use Changes and Land Cover Changes in the Upper Huaihe River Basin, China. *J. Hydrol. Eng.* **2012**, *17*, 800–806. [CrossRef]

39. Zhang, Q.; Bao, W.M.; Chen, W.D.; Shen, D.D. Parameter Estimation Method Based on Parameter Function Surface to Evaluate Runoff Changes in Response to Land Use Changes in Dapoling Watershed. *China Rural Water Hydropower* **2015**, *5*, 49–52.

40. Keesstra, S.; Temme, A.; Schoorl, J.; Visser, S. Evaluating the hydrological component of the new catchment-scale sediment delivery model LAPSUS-D. *Geomorphology* **2014**, *212*, 97–107. [CrossRef]

41. Zhao, R. *Watershed Hydrological Modeling*; Water Conservancy and Electric Power Press: Beijing, China, 1984.

42. Li, Z.; Yao, C.; Zhang, Y.; Qian, X.U.; Huang, Y. Study on grid-based Xinanjiang model. *J. Hydroelectr. Eng.* **2009**, *28*, 25–34. [CrossRef]

43. Zhao, R.; Wang, P. The analysis of Xinanjiang model parameters. *J. China Hydrol.* **1988**, *6*, 4–11.